Human-Exoskeleton Kinematic Calibration to Improve Hand Tracking for Dexterous Teleoperation

Haiyun Zhang[1], Stefano Dalla Gasperina[1], Saad N. Yousaf[1],
Toshimitsu Tsuboi[2], Tetsuya Narita[2], and Ashish D. Deshpande[1,3]

Abstract—**Hand exoskeletons are critical tools for dexterous teleoperation and immersive manipulation interfaces, but achieving accurate hand tracking remains a challenge due to user-specific anatomical variability and donning inconsistencies. These issues lead to kinematic misalignments that degrade tracking performance and limit applicability in precision tasks. We propose a subject-specific calibration framework for exoskeleton-based hand tracking that uses redundant joint sensing and a residual-weighted optimization strategy to estimate virtual link parameters. Implemented on the MAESTRO exoskeleton, our method improves joint angle and fingertip position estimation across users with varying hand geometries. We introduce a data-driven approach to empirically tune cost function weights using motion capture ground truth, enabling more accurate and consistent calibration across participants. Quantitative results from seven subjects show substantial reductions in joint and fingertip tracking errors compared to uncalibrated and evenly weighted models. Qualitative visualizations using a Unity-based virtual hand further confirm improvements in motion fidelity. The proposed framework generalizes across exoskeleton designs with closed-loop kinematics and minimal sensing, and lays the foundation for high-fidelity teleoperation and learning-from-demonstration applications.**

Index Terms—**Hand Tracking, Hand Exoskeleton, Dexterous Manipulation, Kinematics.**

I. INTRODUCTION

Achieving human-level dexterity in robotic manipulation remains a key challenge [1], as current systems still fall short in achieving the versatility needed for tool use and fine manipulation [2], [3].

Dexterous teleoperation, where humans remotely control robotic hands, offers a promising pathway toward this goal. It is essential for applications such as robotic surgery, space exploration, and disaster response, as well as for collecting high-quality demonstrations to train robots via imitation learning [4]. In both real-time control and demonstration settings, the effectiveness of teleoperation hinges on accurately capturing the user's hand movements, driving growing interest in evaluating and improving hand tracking methods for these applications.

Current approaches fall into two main categories: vision-based systems and wearable devices [5], [6]. Vision-based methods, including optical motion capture and camera-based frameworks like MediaPipe [7], offer non-invasive, real-time
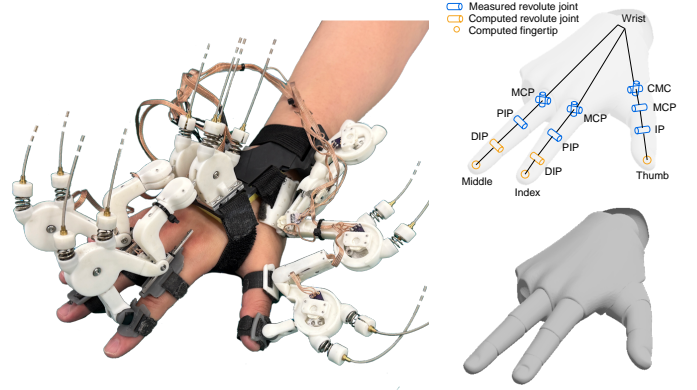
Fig. 1: (Left) The MAESTRO hand exoskeleton worn on the thumb, index, and middle fingers. (Right) Simplified kinematic model of the exoskeleton and corresponding rendering of the mapped virtual hand.

tracking and can achieve sub-centimeter fingertip precision under ideal conditions. However, they remain sensitive to occlusions, lighting variability, and camera placement, which compromises tracking stability and usable workspace [8]. Additionally, they lack haptic feedback, making them less suitable for force-sensitive teleoperation tasks [9].

In contrast, wearable devices——such as sensorized gloves and hand exoskeletons——offer a more direct means of capturing finger motion through joint angle or fingertip sensing [10]. Among these, hand exoskeletons are particularly effective in cluttered or occlusion-prone environments [6], [11], and can deliver haptic feedback to keep users actively engaged during dexterous teleoperation [12]. However, exoskeletons face a persistent challenge in maintaining anatomically accurate tracking across diverse users and donning conditions [13]. Variability in hand size, donning inconsistencies, and slippage at the skin–device interface often introduce kinematic misalignments that degrade tracking accuracy and cause discomfort or unintended interaction forces [14].

To mitigate these issues, prior work has employed redundant passive mechanisms [15]–[17] or underactuated fingertip-only designs [18], [19]. While these designs enable self-alignment to accommodate donning variability, they do not guarantee accurate joint-level tracking. The introduced kinematic redundancy breaks the one-to-one mapping between exoskeleton and anatomical joints, making the system sensitive to slippage, donning variability, and hand size. As a result, even with high-quality sensors, the estimated joint angles can diverge from the user's true finger posture, making precise hand tracking difficult [20].

To address this gap, we propose a subject-specific calibration framework aimed at reducing hand tracking error in exoskeleton-based telemanipulation. Our method estimates virtual link parameters that account for different hand sizes and donning conditions, thereby improving the accuracy of hand tracking across users.

Specifically, we implement and validate this approach on the MAESTRO hand exoskeleton , shown inFig. 1, which employs closed-loop four-bar linkages for passive self-alignment. While this design improves comfort and wearability, it also introduces kinematic redundancy, making the system highly sensitive to hand size, hand anatomy, slippage, and donning conditions [14]. Our proposed calibration mitigates these effects by optimizing virtual link lengths and weighting factors to align exoskeleton outputs with anatomical motion. To address these challenges, we introduce a subject-specific, data-driven calibration framework that aligns exoskeleton outputs with anatomical motion by optimizing virtual link lengths and residual weightings. Instead of relying on rigid hardware alignment, the method estimates these parameters from user motion data, compensating for variations in hand size, finger proportions, and donning configuration.

The calibration is formulated as an optimization problem that minimizes tracking error via a residual-weighted cost function combining joint and fingertip errors. We further introduce a data-driven approach to optimize these weights, enabling the calibration to adapt to subject-specific biomechanics and sensor contributions. This integrated strategy leads to more accurate hand posture estimation and improved tracking fidelity. We implement and evaluate the framework on the MAESTRO hand exoskeleton, demonstrating consistent improvements in joint and fingertip tracking across seven participants with diverse hand geometries. The method is validated both quantitatively and qualitatively, using a virtual hand model rendered in Unity to assess visual plausibility in teleoperation.

Our key contributions are: (i) a subject-specific calibration procedure for virtual link estimation under anatomical and donning variability; (ii) a residual-weight optimization method that enhances tracking accuracy over traditional uniform weighting; and (iii) a comprehensive multi-subject evaluation and virtual validation demonstrating improved fidelity for teleoperation. Together, these contributions establish a generalizable calibration framework for improving exoskeleton-based hand tracking. While demonstrated on MAESTRO, the method applies broadly to other wearable hand exoskeletons with kinematic misalignment or minimal sensing, supporting high-fidelity control in teleoperation and learning-from-demonstration applications.

II. METHODS

A. Hardware Platform

The MAESTRO hand exoskeleton, shown in Fig.1, is used in this study as a representative case to present and validate our subject-specific calibration framework. MAESTRO enables motion tracking and haptic feedback for the thumb, index, and middle fingers via a cable-driven [21], [22]. It includes 8 active and 8 passive joints, each instrumented with rotary potentiometers for joint sensing. The index and middle fingers are each equipped with 5 sensors (2 providing redundant measurements), while the thumb has 6 sensors, including two redundant ones. As shown in the figure, the system can measure or estimate the MCP and PIP joints for the fingers, and the CMC, MCP, and IP joints for the thumb. The distal interphalangeal (DIP) joints are computed from the PIP joints using established biomechanical correlations.

B. Kinematic Model

Each digit of the MAESTRO hand exoskeleton is modeled independently using a dedicated kinematic chain, reflecting the modular mechanical design of the device. These models define the mapping from exoskeleton joint measurements to anatomical joint angles.

The thumb and fingers differ in mechanical structure but share several underlying kinematic equations. As shown in Fig. 2, each digit consists of multiple four-bar closed-loop chains—two for the index and middle fingers, and three for the thumb. All digits follow a common layout: an initial RRPR loop, followed by one (index/middle) or two (thumb) RRRR loops. For each loop, the anatomical joint angle is estimated by modeling the combined kinematics of the exoskeleton linkages, finger segments, and virtual links.

In the following, we present the human–exoskeleton kinematic model, which maps the exoskeleton's sensorized joint angles to estimated human joint angles. For the thumb, the sensorized exoskeleton joint angles are denoted as $(\alpha_2, \beta_2, \gamma_2, \delta_1, \delta_2, \delta_3)$, and the corresponding anatomical joint angles are $(\theta_1, \theta_2, \theta_3)$, representing the CMC, MCP, and IP joints, respectively. While similar models apply to the thumb, index, and middle fingers, here we only detail the thumb model for clarity. Complete loop equations and joint mappings are provided in Fig. 2 and Tab. I.

Using known geometric parameters, the input angles yield intermediate link angles through closed-form trigonometric expressions, as derived in Eqs. 4–6. Due to the RRPR structure of the first loop, the distances d_1 and c_2 are also functions of α_2. The analytical solutions are derived using sum-to-product trigonometric identities for compactness.

As mentioned above, the exoskeleton includes redundant sensor inputs, which can also be derived from the geometry of the kinematic loops. These redundant joint angles are incorporated into the calibration cost function to improve estimation accuracy. Here, δ_1, δ_2, and δ_3 represent redundant joint angles derived from specific four-bar link constraints, as shown in Fig. 2.

Each redundant joint encodes constraints across one or more loops: i) $\hat{\delta}_1$ is defined as the angle between links b_1 and d_2 and depends on both the first and second loops; ii) $\hat{\delta}_2$, defined as the angle between a_2 and the projection of b_2 along the y-axis (y_3), is specific to the index and middle fingers and is influenced by the second loop geometry, $f(\beta)$; and iii) $\hat{\delta}_3$ the angle between a_2 and d_3 is unique to the thumb, and depends on both the second and third loops, $f(\beta, \gamma)$.

These estimated redundant angles are computed using geometric constraints, as:

(a) Thumb Kinematic Model
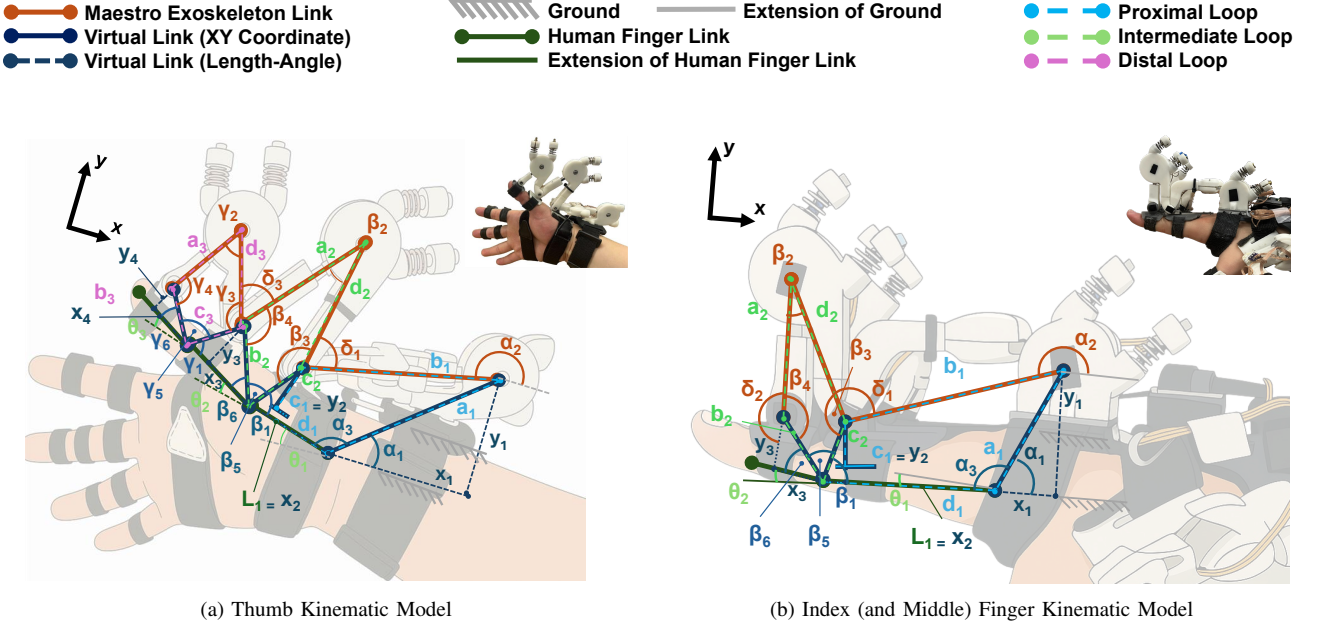
(b) Index (and Middle) Finger Kinematic Model

Fig. 2: Kinematic diagram showing the four-bar mechanisms implemented in the human-robot kinematic model of the MAESTRO hand exoskeleton. (a) The thumb uses three kinematic loops, whereas (b) the index and middle fingers use two kinematic loops. The first loop is an RRPR mechanism, and both the second and third loops are RRRR mechanisms. Specific definitions of each variable are provided in Tab. I.

$$\hat{\delta}_1 = 2\pi + \theta_1 + \beta_1 - \alpha_2 - \beta_3 \tag{1}$$

$$\hat{\delta}_2 = 2\pi - \beta_4 - (\pi/2 - \beta_5) \tag{2}$$

$$\hat{\delta}_3 = 2\pi - \beta_4 - (\pi/2 - \beta_6) - \gamma_3 - (\pi/2 - \gamma_1) \tag{3}$$

where the intermediate variables are presented in Tab. I.

While the kinematic model defines a consistent mapping from exoskeleton to anatomical joints, this mapping is sensitive to inter-subject variability such as hand anatomy, size, and donning configuration. These factors influence the virtual link geometry and can introduce tracking inaccuracies if left uncalibrated. The following section analyzes how variations in key kinematic parameters affect tracking performance, motivating the need for a subject-specific calibration framework.

C. Kinematic Parameters Sensitivity Analysis

To motivate the need for a calibration procedure that adjusts the kinematic parameters values, we first analyzed the sensitivity of fingertip position to perturbations in the virtual link parameters. Using the kinematics model of the index finger, each of the six 2D virtual link coordinates $\{x_1, y_1, x_2, y_2, x_3, y_3\}$ was perturbed independently in simulation, and the resulting deviation in fingertip position was computed. The goal was to demonstrate that even small errors in these parameters can lead to significant inaccuracies in fingertip tracking, thereby justifying the need for precise calibration.

The results, shown in Fig. 3, indicate that proximal parameters—particularly x_1 and x_3—have a significantly larger effect on fingertip position than more distal ones such as y_1 and y_3. This confirms that small errors in estimating virtual link parameters can lead to substantial errors in fingertip
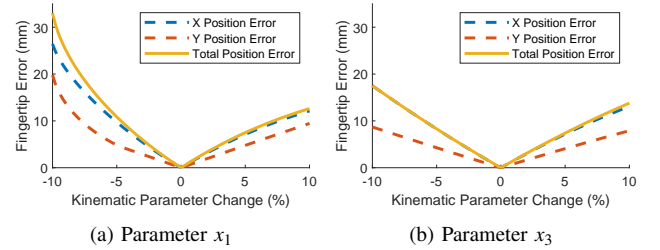

(a) Parameter x_1

(b) Parameter x_3

Fig. 3: Sensitivity analysis in simulation of fingertip position error (mm) as a function of perturbations in select parameters (% variation).

position—up to 30 mm for just a 10% perturbation in proximal coordinates.

Furthermore, due to the kinematic design, variations in horizontal parameters (i.e., x values) tend to produce larger fingertip tracking errors than equivalent changes in vertical ones (y values). This is particularly relevant given that horizontal sliding of the device on the back of the hand is more likely than vertical shifting during wear. Such horizontal misalignments directly impact the inferred finger pose, emphasizing the need for personalized calibration of virtual link positions to maintain accurate fingertip estimation.

D. Human-Exoskeleton Kinematic Calibration

Accurate hand tracking in exoskeletons like MAESTRO is challenging due to non-anatomical joint mappings and user-specific virtual links. These links vary with hand size and donning and cannot be directly measured. We address this by calibrating them from motion data to improve tracking.

The goal of the calibration process is to optimize subject- and donning-specific virtual link parameters (e.g., a_1, c_1, b_2, c_3) by minimizing discrepancies between estimated ($\hat{\theta}_n$, $\hat{\delta}_n$)

Proximal Loop (thumb and index)	Intermediate Loop (thumb and index)	Distal Loop (thumb only)
Input: α_2 **Parameters:** $a_1, b_1, c_1, L_1, \alpha_1$ **Variables:** d_1, α_3 **Output:** θ_1	**Input:** $\beta_2, \delta_1, \delta_2$ **Parameters:** a_2, b_2, d_2, β_6 **Variables:** $c_2, \beta_1, \beta_3, \beta_4, \beta_5$ **Output:** $\theta_2, \hat{\delta}_1, \hat{\delta}_2$	**Input:** γ_2, δ_3 **Parameters:** $a_3, b_3, c_3, d_3, \gamma_1, \gamma_6$ **Variables:** γ_3, γ_5 **Output:** $\theta_3, \hat{\delta}_3$
Solution: $\theta_1 = -\pi + \alpha_3 \qquad (4)$	**Solution:** $\theta_2 = \beta_1 + \beta_5 + \beta_6 - \pi \qquad (5)$	**Solution:** $\theta_3 = \gamma_1 + \gamma_5 + \gamma_6 - \pi \qquad (6)$

Where:

$$d_1 = \sqrt{a_1^2 + b_1^2 - c_1^2 + 2a_1 b_1 \cos(\alpha_2 - \alpha_1)}$$

$$\alpha_3 = -2\arctan\left(\frac{\begin{array}{c} b_1 - 2d_1 + 2a_1\cos(\alpha_2)\cos(\alpha_1) \\ +2(b_1 - d_1)\cos(\alpha_2) + 2a_1\cos(\alpha_1) \\ +b_1\cos(2\alpha_2) \end{array}}{(2\cos(\alpha_2)+1)\cdot(-c_1 + a_1\sin(\alpha_1) + b_1\sin(\alpha_2))} \right)$$

Where:

$$c_2 = \sqrt{c_1^2 + (L_1 - d_1)^2}$$

$$\beta_1 = \arctan\left(\frac{c_1}{L_1 - d_1}\right)$$

$$\beta_3 = \arcsin\left(\frac{a_2 \sin(\beta_2)}{\sqrt{a_2^2 + d_2^2 - 2a_2 d_2 \cos(\beta_2)}}\right)$$

$$\beta_4 = \arccos\left(\frac{c_2^2 + d_2^2 - (a_2^2 + b_2^2) - 2c_2 d_2 \cos(\beta_2)}{-2a_2 b_2}\right)$$

$$\beta_5 = \arccos\left(\frac{a_2^2 + d_2^2 - (b_2^2 + c_2^2) - 2a_2 d_2 \cos(\beta_2)}{-2b_2 c_2}\right)$$

$$+ \arcsin\left(\frac{b_2 \sin(\beta_6)}{\sqrt{b_2^2 + c_2^2 - 2b_2 c_2 \cos(\beta_6)}}\right)$$

Where:

$$\gamma_3 = \arcsin\left(\frac{a_3 \cdot \sin(\gamma_2)}{\sqrt{a_3^2 + d_3^2 - 2a_3 d_3 \cos(\gamma_2)}}\right) +$$

$$+ \arcsin\left(\frac{b_3 \cdot \sin(\gamma_5)}{\sqrt{b_3^2 + c_3^2 - 2b_3 c_3 \cos(\gamma_5)}}\right)$$

$$\gamma_5 = \arccos\left(\frac{a_3^2 + d_3^2 - (b_3^2 + c_3^2) - 2a_3 d_3 \cdot \cos(\gamma_2)}{-2b_3 c_3}\right)$$

TABLE I: Summary of closed-loop kinematic models for computing human finger joint angles from exoskeleton sensor inputs. Each loop models one anatomical joint, using a single exoskeleton joint angle as input and incorporating exoskeleton linkages, anatomical finger segments, and virtual link lengths. The 1st and 2nd loops are used for the index, middle, and thumb digits; the 3rd loop is unique to the thumb.
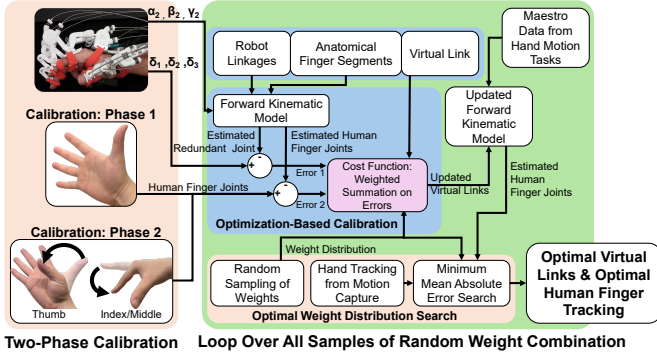

Fig. 4: Visualization of the kinematic parameter calibration with weighted optimization. The human user performs a two-phase calibration, and the weight distribution is adjusted based on human data.

and measured joint angles ($\delta_{n,\text{ref}}$) or known configurations ($\theta_{n,\text{ref}}$). The inputs to the calibration are the measured joint angles, while the outputs are the estimated virtual links, which generate updated estimates of the user's joint angles.

The full procedure, illustrated in Fig. 4, consists of two phases:

In phase one (ϕ_1), subjects fully extend their fingers to form a flat-hand posture and hold it for a few seconds while static joint measurements are recorded. This configuration imposes known anatomical constraints, which serve as reference angles (θ_{ref} and δ_{ref}) for calibration: all finger joints are assumed to be at $0°$, except for the thumb CMC flexion/extension, which is anatomically set at $70°$.

In phase two (ϕ_2), subjects perform isolated flexion of the MCP joints of the thumb, index, and middle fingers while keeping the IP (thumb) and PIP (index/middle) joints extended. In this case, the reference angles for the MCP joints

are unknown and serve as targets for optimization, while the IP/PIP joints are again assumed to remain at $0°$.

The two-phase protocol enables global alignment through the flat-hand posture and enforces dynamic consistency via isolated MCP flexion. Together, these conditions provide complementary constraints that help the calibration generalize across configurations. An optimization routine then updates the virtual link parameters by minimizing the discrepancy between measured redundant joint angles (or reference postures) and those predicted by the kinematic model.

There are two interchangeable representations of virtual link parameters: the length–angle form ($a_1, \alpha_1, c_2, \beta_1, b_2, \beta_6, b_3, \gamma_6$), used in the kinematic model, and the XY-coordinate form ($x_1, y_1, x_2, y_2, x_3, y_3, x_4, y_4$), used as input for optimization. The conversion between the two is done via trigonometric identities. We adopt the length–angle form for computing joint angles using closed-form geometric relations, and the XY-coordinate form for optimization due to its dimensional consistency.

The calibration cost function is defined as a weighted sum of squared errors between estimated joint angles and either known reference or redundant sensor readings, respectively for phase one and two. We define each error term Δ as the discrepancy between the model and ground truth, as follows:

$$\Delta\theta_{n,\phi_n}^{(i)} = \hat{\theta}_n^{(i)} - \theta_{n,\text{ref}} \qquad (7)$$

for anatomical joints with known reference, where the superscript i identifies samples over the calibration period, n is the joint index, ϕ_n is the calibration phase, and θ_{ref} is the measured or known reference angle (e.g., $0°$ during hand flattening)

$$\Delta\delta_{n,\phi_n}^{(i)} = \hat{\delta}_n^{(i)} - \delta_{n,\text{ref}}^{(i)} \qquad (8)$$

for redundant joints with angular sensors, where δ_{ref} is the reference angle measured by the redundant sensors.

For the index and middle fingers, the cost function is:

$$f_1(\mathbf{x}) = \frac{1}{N}\sum_{i=1}^{N}\Big(w_1(\Delta\theta_{1,\phi_1}^{(i)})^2 + w_2(\Delta\theta_{2,\phi_1}^{(i)})^2 + w_3(\Delta\delta_{1,\phi_1}^{(i)})^2 + \\ w_4(\Delta\delta_{2,\phi_1}^{(i)})^2 + w_5(\Delta\theta_{2,\phi_2}^{(i)})^2 + w_6(\Delta\delta_{1,\phi_2}^{(i)})^2 \Big) \qquad (9)$$

where $\mathbf{x} = (x_1, y_1, x_2, y_2, x_3, y_3)$, w_k are weights and N is the number of samples. To ensure a well-posed optimization, the number of error terms must match the number of virtual link parameters. For example, six parameters require six independent error terms. While both $\Delta\delta_{1,\phi_2}$ and $\Delta\delta_{2,\phi_2}$ are valid choices, we empirically found that using $\Delta\delta_{1,\phi_2}$ results in better calibration.

Similarly, the cost function of the thumb is defined as:

$$f_2(\mathbf{y}) = \frac{1}{N}\sum_{i=1}^{N}\Big(w_1(\Delta\theta_{1,\phi_1}^{(i)})^2 + w_2(\Delta\theta_{2,\phi_1}^{(i)})^2 + w_3(\Delta\theta_{3,\phi_1}^{(i)})^2 + \\ w_4(\Delta\delta_{1,\phi_1}^{(i)})^2 + w_5(\Delta\delta_{2,\phi_1}^{(i)})^2 + w_6(\Delta\theta_{3,\phi_2}^{(i)})^2 + \\ w_7(\Delta\delta_{1,\phi_2}^{(i)})^2 + w_8(\Delta\delta_{2,\phi_2}^{(i)})^2 \Big) \qquad (10)$$

where $\mathbf{y} = (x_1, y_1, x_2, y_2, x_3, y_3, x_4, y_4)$. Subsequently, the global optima of the two problems are obtained as:

$$\mathbf{x}^* = \arg\min_{\mathbf{x}} f_1(\mathbf{x}), \quad \mathbf{y}^* = \arg\min_{\mathbf{y}} f_2(\mathbf{y}) \qquad (11)$$

The kinematic calibration procedure relies on optimizing a set of virtual link parameters by minimizing a weighted sum of joint angle errors. The performance of this optimization depends not only on the quality of the input data but also on how the error terms are weighted in the cost function. While the simulation-based sensitivity analysis, presented in II-C, offers a first-principles rationale for prioritizing proximal parameters, it does not capture real-world factors such as model inaccuracies and inter-subject variability. To address this, we conducted a data-driven weight refinement via motion capture validation (see Section III-A).

III. HUMAN-SUBJECT EXPERIMENTS

Human-subject experiments were conducted to empirically optimize the calibration cost function weights and evaluate hand tracking performance. The study was approved by the Institutional Review Board (IRB ID: STUDY00002527). Seven participants with varying hand sizes (Table II) wore the exoskeleton and completed the protocol shown in Fig. 5. Reflective markers were placed on anatomical landmarks of the thumb and index finger for motion capture, as shown in Fig. 5a- 5b.

First, participants performed the two-phase calibration routine: (i) full finger extension and (ii) MCP flexion of the thumb, index, and middle fingers with IP/PIP joints extended, as described in Sec. II-D. These postures provided constrained joint trajectories for estimating subject-specific kinematic parameters.

Second, during the hand tracking task, participants performed three representative finger motions: (i) combined thumb MCP and IP flexion, (ii) index MCP flexion with PIP extended, and (iii) combined index MCP and PIP flexion, as shown in Fig. 5. Each participant performed six trials per motion. These motions were selected to isolate individual joint estimation performance. MAESTRO sensor data and motion capture trajectories were recorded simultaneously and synchronized during post-processing. Due to limited visibility and occlusion when wearing the device, the analysis was limited to MCP and IP joints of the thumb, and MCP and PIP joints of the index finger. Due to the shared mechanical and kinematic design between the index and middle fingers, the results obtained for the index finger can also be applied to the middle finger.

A. Quantitative Analysis

Optimal Weight Search: To enhance calibration robustness against modeling uncertainties and local minima, cost function weights (w_k) were empirically optimized using a data-driven approach. Each subject performed dynamic finger movements while wearing the MAESTRO exoskeleton, and joint angle estimates were compared to ground-truth trajectories. For each subject, 500 candidate weight combinations ($w_k \in [0, 10]$) were randomly sampled across all cost function dimensions. Each weight distribution was used to calibrate virtual link parameters from the two-phase calibration data, and compute the corresponding joint angles and fingertip positions. Motion capture trajectories served as ground truth to identify the weights that minimize the mean absolute error (MAE) in joint angle tracking. The weight distribution yielding the lowest error per subject was selected as optimal. Final weights were obtained by averaging these optimal weights across all participants and applied consistently in subsequent analyses.

Performance Validation: Using the averaged optimal weights, each participant's virtual link parameters were calibrated based on their two-phase calibration data. The resulting optimized kinematic model was used to estimate joint angles from MAESTRO sensor measurements during dynamic tasks. These estimates were quantitatively validated against motion capture ground truth by computing the mean absolute error (MAE) per joint, averaged across repetitions and subjects.

B. Qualitative Analysis

After verifying the quantitative performance of our exoskeleton-based hand tracking system, we qualitatively assessed how well the calibrated virtual hand resembled the user's real hand motion in a virtual environment. A custom Unity hand model was developed using direct linear joint-to-joint mapping from the MAESTRO-estimated angles. DIP joints were inferred from corresponding PIP angles via biomechanical coupling, and all other joints were fixed. The visualization used anatomically plausible joint limits and averaged bone lengths across subjects and conditions, to isolate the effect of calibration. Participants reproduced representative static and dynamic hand gestures——such as pinching and grasping——under calibrated and uncalibrated conditions. These gestures were used to generate side-by-side visualization for offline inspection.

(a) Thumb markers   (b) Index markers
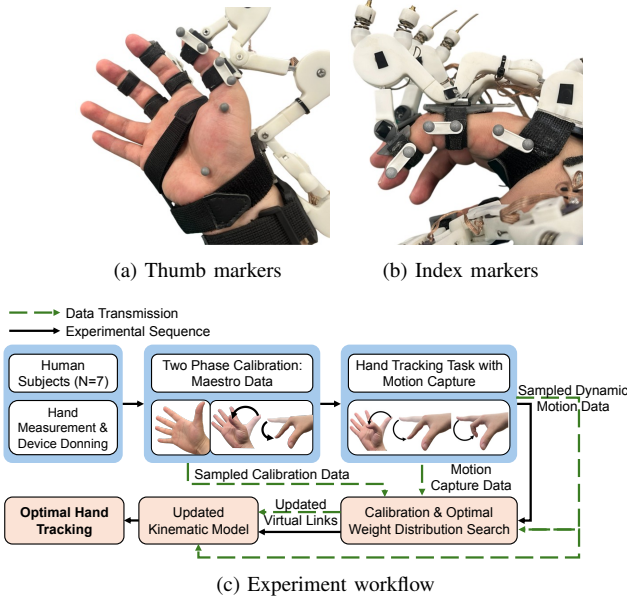

(c) Experiment workflow

Fig. 5: Experimental setup showing motion capture markers placed on the (a) thumb and (b) index finger, along with (c) the experiment workflow for human subject testing.

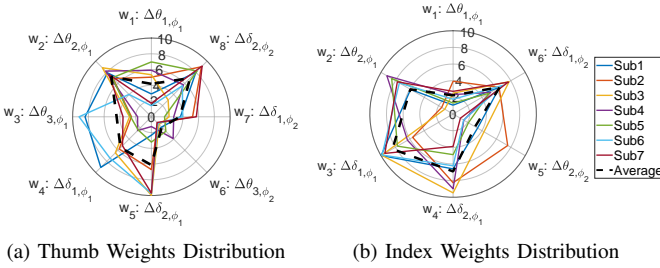(a) Thumb Weights Distribution   (b) Index Weights Distribution

Fig. 6: Subject-specific optimized weights distributions for thumb and index finger calibration. The dashed black line represents the averaged distribution across all subjects.

IV. RESULTS

A. Quantitative Results

Optimal Weight Search: The cost function weights used in the calibration routine is search by averaging the individual optimal weights distribution. The individual optimal weights-distribution is from each subject by minimizing the joint angle mean absolute error relative to motion capture ground truth. The individual weight distributions for both the thumb and index fingers across all seven subjects, along with the averaged optimal weights, are shown in Fig. 6. While the individual profiles exhibit broadly consistent contours, indicating robustness in the optimal weights distribution, some outliers are observed. These deviations likely stem from subject-specific differences in hand size, donning variability, or movement variability during the calibration trials. The averaged results for the thumb (Fig.6a) indicate higher optimal weights for w_2 and w_8, suggesting that the calibration is more sensitive to parameters contributing to θ_2 and δ_2, both related to the thumb MCP joint. In contrast, the index finger results (Fig.6b) show greater weights for w_3 and w_4, highlighting the sensitivity of the calibration to δ_1 and δ_2, associated with the PIP joints of the index and middle fingers. Overall, the optimized weights emphasize the second kinematic loop parameters—particularly

Subject	Length [cm]	Width [cm]	Size	Joint MAE ↓ [%]				Tip MAE ↓ [%]	
				T-MCP	T-IP	I-MCP	I-PIP	Thumb	Index
1	17.0	6.5	S	−8.5	64.7	53.5	64.3	32.2	69.0
2	17.2	8.0	S–M	−39.5	11.4	70.8	44.2	5.3	60.7
3	18.0	9.5	M–L	−6.6	12.5	−40.5	57.0	32.1	58.0
4	18.5	9.0	M	33.6	48.6	−3.1	61.7	25.2	63.8
5	17.0	8.5	M	−18.4	3.2	64.2	43.9	41.2	85.2
6	19.2	9.8	L	59.1	66.1	73.6	56.4	72.1	83.3
7	18.1	7.8	M	−10.8	62.1	57.2	35.4	3.0	66.0
Avg	**17.6**	**8.4**	**–**	**37.1**	**56.7**	**68.3**	**52.9**	**34.8**	**71.5**

TABLE II: Hand dimensions (Length, Width in cm) and percent reduction in joint and fingertip tracking errors after calibration.

the thumb MCP and finger PIP joints—as key contributors to accurate hand tracking.

Performance Validation: We report mean absolute errors (MAE) between the MAESTRO-based tracking and ground truth for joint angles and fingertip positions. Average results are shown in Fig. 7, while subject-specific results for the three tracking tasks are shown in Fig. 8. Optimal-weighted calibration consistently achieved the lowest MAE, followed by the even-weighted calibration, with the uncalibrated model exhibiting the highest error. This trend holds across joints for the tested digits, validating the benefit of subject-specific weight optimization.

Table II summarizes the results, showing joint-wise and fingertip position error reductions across all participants. Despite some variability across joints and subjects, calibration consistently led to notable reductions in both joint and fingertip tracking errors. The greatest improvements were observed in the thumb IP and index PIP joints, as well as in the fingertip position of the index finger. Fingertip position accuracy improved similarly, with the index fingertip achieving the highest average error reduction (71.5%), while the thumb fingertip showed a more moderate improvement (34.8%). These gains support the calibration's effectiveness in enhancing end-effector representation, which is especially relevant for precision manipulation tasks.

Overall, the index finger showed the most consistent improvements across subjects, particularly in PIP joint tracking and fingertip accuracy. The thumb also benefited from calibration, though with greater variability—likely due to anatomical differences and higher articulation complexity. A few negative joint error reductions (i.e., increases in error post-calibration) were observed in the thumb MCP and index MCP joints for certain subjects, possibly due to residual alignment errors during marker placement or mechanical coupling not fully captured by the model. Despite inter-subject variability, the averaged error reductions and similarity in weight profiles suggest that the calibration method generalizes well across users with different hand sizes.

To illustrate the method's performance, Fig. 9 shows tracking results for *Subject 6* across thumb and index. The weighted calibration consistently produces trajectories that align more closely with the ground truth data, compared to both the uncalibrated and even-weighted baselines. This subject serves as a representative example of the effectiveness of our approach in reducing tracking error in dynamic finger motion.
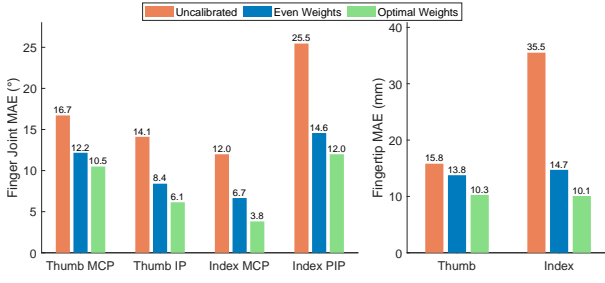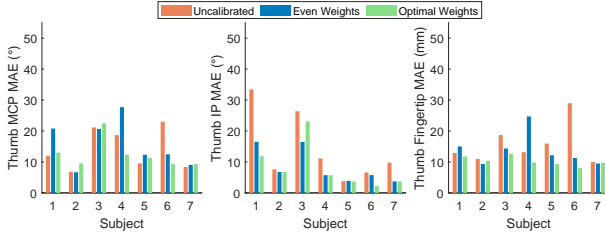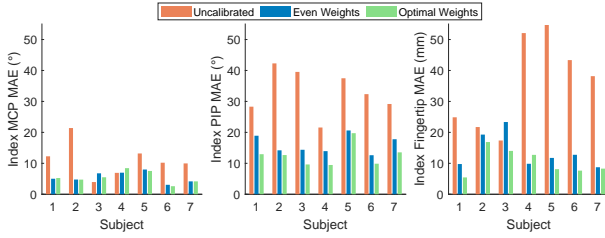
Fig. 7: Hand tracking accuracy results averaged across 7 subjects and all tasks, shown for (left) joint angles (thumb MCP, thumb IP, index MCP, index PIP) and (right) fingertip position (thumb, index).

(a) Combined Thumb MCP and IP Flexion

(b) Combined Index MCP and IP Flexion

Fig. 8: Hand tracking accuracy results for 7 subjects. (a) Thumb joint angles and fingertip errors across all subjects. (b) Index joint angles and fingertip errors across all subjects for two different index finger motions.

B. Qualitative Results

To qualitatively assess improvements in hand tracking, we visualized hand tracking results using a virtual Unity hand driven by joint estimates under both calibrated and uncalibrated conditions. Representative postures (e.g., pinch, grasp) were recorded for each subject and used to qualitatively assess tracking fidelity. As shown in Fig. 10, orange hands depict postures based on uncalibrated data, while green hands reflect calibrated estimates.

Calibration leads to visibly improved alignment with the real hand, particularly in fine thumb and finger articulations. These visualizations qualitatively confirm the enhanced motion fidelity achieved through the proposed subject-specific calibration. A demonstration of the real-time virtual hand motion tracking is provided in the supplementary video.

V. DISCUSSION AND CONCLUSION

This study introduced a subject-specific calibration framework to enhance hand tracking accuracy with a sensorized robotic exoskeleton. The method yielded consistent improvements in both joint angle and fingertip tracking across participants with varying hand sizes and donning conditions.
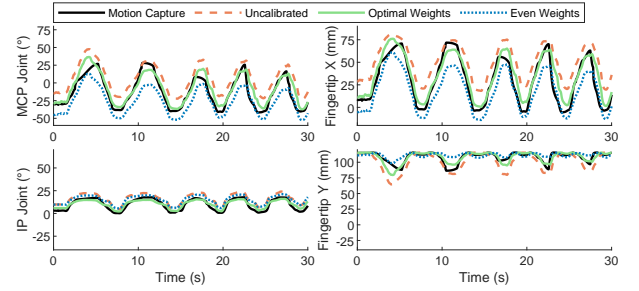
(a) Combined Thumb MCP and IP flexion
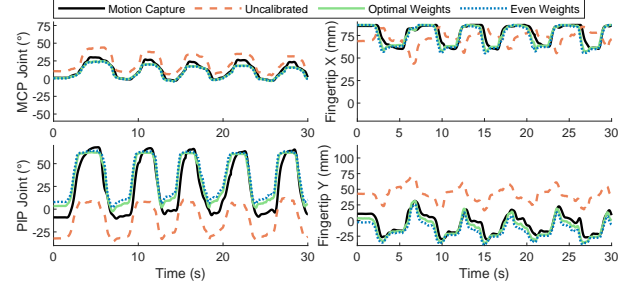
(b) Combined Index MCP and PIP flexion

Fig. 9: Comparison of hand tracking performance for *Subject 6*. Each subplot compares trajectories obtained from motion capture, uncalibrated tracking, and calibration with even and optimal weights.

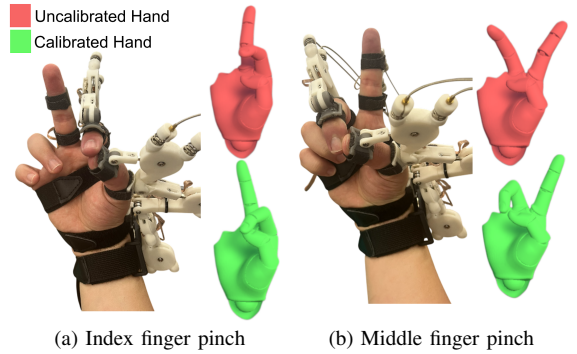(a) Index finger pinch   (b) Middle finger pinch

Fig. 10: Real and virtual hands (Unity rendering) shown side by side for uncalibrated (red) and calibrated (green) tracking.

We also introduced an optimal weight distribution for the calibration process, which consistently outperformed even-weighted calibration, particularly in joints affected by closed-loop kinematics. These results suggest that inaccuracies in virtual link parameters, originated from user-specific fit, can significantly affect tracking and should be explicitly calibrated. In a few cases, such as Subject 3, improvements were not observed, likely due to external factors like motion capture occlusion or soft tissue artifacts. Moreover, when initial tracking errors were already low, optimization converged near a local minimum, yielding marginal or oscillatory improvements.

When compared to existing tracking systems, our method demonstrated competitive performance. Markerless vision-based methods often report fingertip errors exceeding 10–20mm [23], while our calibrated system achieves fingertip MAE of 10mm—sufficient for teleoperation applications [12]. Compared to other exoskeleton-based approaches that rely on structured calibration routines [24], our method avoids

constrained motion patterns and demonstrates more robust tracking across users. A key contribution is the validation of performance across a diverse user group, in contrast with prior single-subject evaluations. We also provide both quantitative and qualitative evidence of improved motion plausibility using a Unity-rendered virtual hand.

Importantly, the proposed calibration framework is generalizable. Many hand exoskeletons employ 4-bar linkages or underactuated designs due to the challenge of aligning robotic joints with anatomical joints [15]. These designs require virtual kinematic models whose geometry is affected by unmeasurable donning conditions. Our approach compensates for such inaccuracies by optimizing virtual link lengths to minimize joint estimation error. While additional sensors improve observability and constraint in the optimization, our method is compatible with systems lacking redundancy. By addressing anatomical variability and user-specific fit, this work helps bridge the gap between human intent and virtual or robotic hand motion.

Despite the promising results, this study presents several limitations. First, the evaluation was limited to isolated postures rather than continuous movements, primarily due to motion capture occlusion issues. While this enabled precise joint-level analysis, it did not fully capture the temporal complexity of real-world manipulation tasks. Second, the calibration assumes a consistent exoskeleton fit and stable sensor behavior, yet in practice, variations in donning, long-term use, and environmental conditions may affect performance and reduce calibration validity over time.

In conclusion, this work lays the foundation for extending subject-specific calibration methods to practical teleoperation and robot learning applications. By combining subject-specific virtual links optimization with a quantitative validation, we present a framework to enhance the fidelity of exoskeleton-based hand tracking. Qualitative assessments using a simulated teleoperation hand model confirmed that calibration leads to more anatomically plausible postures, and showed improved visual alignment post-calibration. Although residual joint angle errors remain in the 10-degree range, the resulting motions are visually coherent and consistent. Such improvements in motion fidelity are essential for downstream teleoperation tasks involving fine manipulation, shared autonomy, or learning from demonstration. Future work will focus on evaluating performance in dynamic, task-based scenarios and integrating the framework into imitation learning pipelines to assess its effect on policy generalization and data efficiency.

REFERENCES

[1] J. Zhang, H. Zhao, K. Chen, G. Fei, X. Li, Y. Wang, Z. Yang, S. Zheng, S. Liu, and H. Ding, "Dexterous hand towards intelligent manufacturing: A review of technologies, trends, and potential applications," Robotics and Computer-Integrated Manufacturing, vol. 95, p. 103021, 2025.

[2] C. Yu and P. Wang, "Dexterous manipulation for multi-fingered robotic hands with reinforcement learning: A review," Frontiers in Neurorobotics, vol. 16, p. 861825, 2022.

[3] T. Chen, M. Tippur, S. Wu, V. Kumar, E. Adelson, and P. Agrawal, "Visual dexterity: In-hand reorientation of novel and complex object shapes," Science Robotics, vol. 8, no. 84, p. eadc9244, 2023.

[4] W. Si, N. Wang, and C. Yang, "A review on manipulation skill acquisition through teleoperation-based learning from demonstration," Cognitive Computation and Systems, vol. 3, no. 1, pp. 1–16, 2021.

[5] C. Mizera, T. Delrieu, V. Weistroffer, C. Andriot, A. Decatoire, and J.-P. Gazeau, "Evaluation of hand-tracking systems in teleoperation and virtual dexterous manipulation," IEEE Sensors Journal, vol. 20, no. 3, pp. 1642–1655, 2019.

[6] J. Fu, M. Poletti, Q. Liu, E. Iovene, H. Su, G. Ferrigno, and E. De Momi, "Teleoperation control of an underactuated bionic hand: Comparison between wearable and vision-tracking-based methods," Robotics, vol. 11, no. 3, p. 61, 2022.

[7] A. Vakunov, C.-L. Chang, F. Zhang, G. Sung, M. Grundmann, and V. Bazarevsky, "Mediapipe hands: On-device real-time hand tracking," in Workshop on Computer Vision for AR/VR, vol. 2, p. 5, 2020.

[8] F. Mueller, D. Mehta, O. Sotnychenko, S. Sridhar, D. Casas, and C. Theobalt, "Real-time hand tracking under occlusion from an egocentric rgb-d sensor," in Proceedings of the IEEE international conference on computer vision, pp. 1154–1163, 2017.

[9] H. S. Moon, G. Orr, and M. Jeon, "Hand tracking with vibrotactile feedback enhanced presence, engagement, usability, and performance in a virtual reality rhythm game," International Journal of Human–Computer Interaction, vol. 39, no. 14, pp. 2840–2851, 2023.

[10] T. Du Plessis, K. Djouani, and C. Oosthuizen, "A review of active hand exoskeletons for rehabilitation and assistance," Robotics, vol. 10, no. 1, p. 40, 2021.

[11] K. Darvish, L. Penco, J. Ramos, R. Cisneros, J. Pratt, E. Yoshida, S. Ivaldi, and D. Pucci, "Teleoperation of humanoid robots: A survey," IEEE Transactions on Robotics, vol. 39, no. 3, pp. 1706–1727, 2023.

[12] D. Leonardis, M. Gabardi, S. Marcheschi, M. Barsotti, F. Porcini, D. Chiaradia, and A. Frisoli, "Hand teleoperation with combined kinaesthetic and tactile feedback: A full upper limb exoskeleton interface enhanced by tactile linear actuators," Robotics, vol. 13, no. 8, p. 119, 2024.

[13] K. Xia, X. Chen, X. Chang, C. Liu, L. Guo, X. Xu, F. Lv, Y. Wang, H. Sun, and J. Zhou, "Hand exoskeleton design and human–machine interaction strategies for rehabilitation," Bioengineering, vol. 9, no. 11, p. 682, 2022.

[14] S. N. Yousaf, G. Mukherjee, R. King, and A. D. Deshpande, "Experimental and simulation-based estimation of interface power during physical human-robot interaction in hand exoskeletons," IEEE Robotics and Automation Letters, vol. 9, no. 3, pp. 2575–2581, 2023.

[15] M. Sarac, M. Solazzi, D. Leonardis, E. Sotgiu, M. Bergamasco, and A. Frisoli, "Design of an underactuated hand exoskeleton with joint estimation," in Advances in Italian Mechanism Science: Proceedings of the First International Conference of IFToMM Italy, pp. 97–105, Springer, 2016.

[16] W. Wei, B. Zhou, B. Fan, M. Du, G. Bao, and S. Cai, "An adaptive hand exoskeleton for teleoperation system," Chinese Journal of Mechanical Engineering, vol. 36, no. 1, p. 60, 2023.

[17] H. Zhang, S. Hu, Z. Yuan, and H. Xu, "Doglove: Dexterous manipulation with a low-cost open-source haptic force feedback glove," arXiv preprint arXiv:2502.07730, 2025.

[18] Y. Park, S. Lee, and J. Bae, "Wehaptic-light: A cable slack-based compact hand force feedback system for virtual reality," Mechatronics, vol. 79, p. 102638, 2021.

[19] E. Amirpour, R. Fesharakifard, H. Ghafarirad, S. M. Rezaei, A. Saboukhi, M. Savabi, and M. R. Gorji, "A novel hand exoskeleton to enhance fingers motion for tele-operation of a robot gripper with force feedback," Mechatronics, vol. 81, p. 102695, 2022.

[20] Y. Yun, P. Agarwal, and A. D. Deshpande, "Accurate, robust, and real-time pose estimation of finger," Journal of Dynamic Systems, Measurement, and Control, vol. 137, no. 3, p. 034505, 2015.

[21] P. Agarwal, J. Fox, Y. Yun, M. K. O'Malley, and A. D. Deshpande, "An index finger exoskeleton with series elastic actuation for rehabilitation: Design, control and performance characterization," The International Journal of Robotics Research, vol. 34, no. 14, pp. 1747–1772, 2015.

[22] P. Agarwal, Y. Yun, J. Fox, K. Madden, and A. D. Deshpande, "Design, control, and testing of a thumb exoskeleton with series elastic actuation," The International Journal of Robotics Research, vol. 36, no. 3, pp. 355–375, 2017.

[23] D. Abdlkarim, M. Di Luca, P. Aves, M. Maaroufi, S.-H. Yeo, R. C. Miall, P. Holland, and J. M. Galea, "A methodological framework to assess the accuracy of virtual reality hand-tracking systems: A case study with the meta quest 2," Behavior research methods, vol. 56, no. 2, pp. 1052–1063, 2024.

[24] Y. Su, G. Li, Y. Deng, I. Sarakoglou, N. G. Tsagarakis, and J. Chen, "The joint-space reconstruction of human fingers by using a highly under-actuated exoskeleton," in 2024 IEEE International Conference on Robotics and Automation (ICRA), pp. 9645–9651, IEEE, 2024.